

Experimental setup of NTSC SrII optical lattice clock

Feng Guo(郭峰), Jia-An Li(李家安), Yan-Yan Liu(刘艳艳), Xiao-Tong Lu(卢晓同), and Hong Chang(常宏)
Citation: Chin. Phys. B, 2026, 35 (**2**): 023702. DOI: 10.1088/1674-1056/adecfd
http://cpb.iphy.ac.cn; http://iopscience.iop.org/cpb

What follows is a list of articles you may be interested in

Observation of Josephson effect in ^{23}Na spinor Bose-Einstein condensates

Yong Qin(秦永), Xin Wang(王鑫), Jun Jian(蹇君), Wenliang Liu(刘文良), Jizhou Wu(武寄洲), Yuqing Li(李玉清), Jie Ma(马杰), Liantuan Xiao(肖连团), and Suotang Jia(贾锁堂)
Chin. Phys. B, 2025, 34 (**3**): 033701. DOI: 10.1088/1674-1056/ada42f

Superfluid to Mott-insulator transition in a one-dimensional optical lattice

Wenliang Liu(刘文良), Ningxuan Zheng(郑宁宣), Jun Jian(蹇君), Li Tian(田丽), Jizhou Wu(武寄洲), Yuqing Li(李玉清), Yongming Fu(付永明), Peng Li(李鹏), Vladimir Sovkov, Jie Ma(马杰), Liantuan Xiao(肖连团), and Suotang Jia(贾锁堂)
Chin. Phys. B, 2022, 31 (**7**): 073702. DOI: 10.1088/1674-1056/ac6579

Enhanced cold mercury atom production with two-dimensional magneto-optical trap

Ye Zhang(张晔), Qi-Xin Liu(刘琪鑫), Jian-Fang Sun(孙剑芳), Zhen Xu(徐震), and Yu-Zhu Wang(王育竹)
Chin. Phys. B, 2022, 31 (**7**): 073701. DOI: 10.1088/1674-1056/ac5397

Dynamical properties of ultracold Bose atomic gases in one-dimensional optical lattices created by two schemes

Jiang Zhu(朱江), Cheng-Ling Bian(边成玲), Hong-Chen Wang(王红晨)
Chin. Phys. B, 2019, 28 (**9**): 093701. DOI: 10.1088/1674-1056/ab3448

Strontium optical lattice clock at the National Time Service Center

Ye-Bing Wang(王叶兵), Mo-Juan Yin(尹默娟), Jie Ren(任洁), Qin-Fang Xu(徐琴芳), Ben-Quan Lu(卢本全), Jian-Xin Han(韩建新), Yang Guo(郭阳), Hong Chang(常宏)
Chin. Phys. B, 2018, 27 (**2**): 023701. DOI: 10.1088/1674-1056/27/2/023701

INSTRUMENTATION AND MEASUREMENT

Experimental setup of NTSC SrII optical lattice clock

Feng Guo(郭峰)[1], Jia-An Li(李家安)[1,2], Yan-Yan Liu(刘艳艳)[1], Xiao-Tong Lu(卢晓同)[1,2,†], and Hong Chang(常宏)[1,2,‡]

[1] *National Time Service Center, Chinese Academy of Sciences, Xi'an* 710600, *China*

[2] *School of Astronomy and Space Science, University of Chinese Academy of Sciences (CAS), Beijing* 100049, *China*

(Received 20 May 2025; revised manuscript received 30 June 2025; accepted manuscript online 8 July 2025)

We report the SrII optical lattice clock at the National Time Service Center (NTSC). In this system, a blackbody radiation shield with movable lattice mitigates blackbody radiation shifts through active temperature control. A shallow optical lattice with minimal tunneling minimizes AC Stark shifts. Phase-locked counter-propagating lattice beams and conductive vacuum viewports further reduce systematic uncertainties and a novel initial-state preparation method simplifies the system. Clock transition spectra achieve a linewidth of 2.5 Hz with a 400 ms clock pulse, and self-comparison stability reaches 5.1×10^{-16} at 1 s. These advancements give this clock the potential to be a critical platform for realizing outstanding systematic uncertainties in the future.

Keywords: optical lattice, optical clock, strontium

PACS: 37.10.Jk, 32.70.Jz, 06.30.Ft, 42.62.Eh

DOI: 10.1088/1674-1056/adecfd **CSTR:** 32038.14.CPB.adecfd

1. Introduction

Precise time measurement is a cornerstone of modern physics, with far-reaching implications for fundamental physics, navigation and geodesy.[1] Optical atomic clocks, leveraging electronic transitions in atoms, have surpassed traditional microwave clocks by two to three orders of magnitude in both stability and accuracy.[2–4] Among these, the strontium optical lattice clock developed at JILA has achieved a remarkable systematic uncertainty of 8.1×10^{-19},[5] setting the milestone for neutral-atom clocks. These advancements not only enable precision tests of fundamental physics, including dark matter interactions[6,7] and gravitational redshift predicted by general relativity,[8,9] but also drive efforts to redefine the SI second based on optical transitions.[10–12]

The roadmap towards a redefinition of the second specifies that at least three different optical clocks (either in different laboratories or of different species) have demonstrated validated uncertainties of about two orders of magnitude better than the best Cs atomic clocks of the time, i.e., with an uncertainty below 2×10^{-18}. For most optical lattice clocks, the blackbody radiation (BBR) shift and the lattice light AC Stark shift are the main contributors to systematic uncertainties, and mitigating these shifts is critical for achieving a clock uncertainty of 10^{-19}.[2,4,5,13–17] To address the BBR shift, precise temperature measurements and thermal homogeneity around the atomic ensemble are essential.[5,17] Researchers have demonstrated the effectiveness of techniques such as BBR shield and vacuum chamber temperature stabilization.[8,13,18] For the AC Stark shift, reducing the lattice trap depth below $20E_r$ (where E_r is the lattice photon recoil energy) can significantly suppress this effect, as demonstrated by JILA, which achieved an AC Stark shift uncertainty of 3.5×10^{-19}.[5,19] However, shallow lattices introduce challenges, such as tunneling and decoherence, which can be mitigated by using gravity to lift the degeneracy between the adjacent lattice sites that form 'Wannier–Stark states'.[19,20] Despite these advances, few optical lattice clocks have combined BBR shielding and shallow lattice techniques to achieve systematic uncertainties on the order of 10^{-19}.

In this study, we present the SrII optical lattice clock at NTSC, an upgraded system incorporating a temperature-controlled BBR shield, movable optical lattice, and shallow lattice with minimal tunneling. Additional innovations include a conductive vacuum viewport, phase-locked counter-propagating lattices, a unique initial-state preparation method and a compact optical design. These enhancements collectively reduce systematic uncertainties.

2. Experimental setup

The physical system for cooling and exciting the atoms in the optical clock is illustrated in Fig. 1(a). Specifically, a vacuum oven houses high-purity solid strontium within a ceramic hollow column, surrounded by a multilayered heat shield to optimize the thermal efficiency. A nichrome wire

†Corresponding author. E-mail: luxiaotong@ntsc.ac.cn

‡Corresponding author. E-mail: changhong@ntsc.ac.cn

© 2026 Chinese Physical Society and IOP Publishing Ltd. All rights, including for text and data mining, AI training, and similar technologies, are reserved.

coiled around the column heats the assembly, producing a collimated atomic beam through capillary clusters at the oven aperture. This atomic beam first passes through a 2D optical molasse to reduce the radial divergence angle using a 461 nm collimating beam. Subsequently, the atoms enter a Zeeman slower, interacting with a counter-propagating 461 nm laser to increase the number of low-speed atoms. The slowed atoms then enter a titanium science chamber, assembled with three Conflat flanges with a 35 mm diameter window (CF35) and twenty-four Conflat flanges with a 16 mm diameter window (CF16). The indium tin oxide (ITO) coating on the vacuum side of the viewports enhances the surface conductivity, preventing stray charge accumulation. The surface resistances of the BBR shield's inner oxide layer and the ITO coating were measured to be below 5 kΩ and 40 kΩ, respectively, demonstrating their ability to prevent surface charge accumulation. The vacuum viewports, the BBR shield and the chamber as a whole form a Faraday cage, thereby suppressing DC Stark shifts.[21] The water-cooled anti-Helmholtz coils are positioned symmetrically above and below the chamber to provide the magnetic field for the MOT. Lasers from the optical system are delivered into the physics system via fibers, with standardized screw holes around each window for mounting the caged optical structural elements.

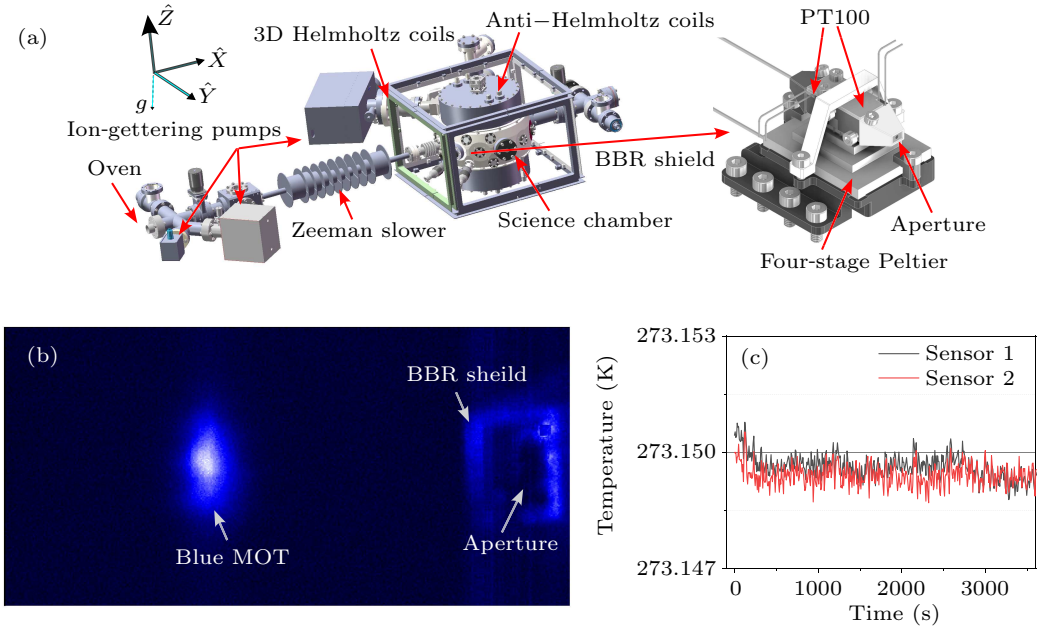


Fig. 1. (a) Schematic of the physics package, integrating an oven, a Zeeman slower, science chamber, magnetic coils and a BBR shield. The system is tilted so that the longitudinal axis of lattice forms a 75° with gravity. (b) Blue magneto-optical trap (MOT) is imaged with an electron-multiplying charge-coupled device (EMCCD), and the aperture of the BBR shield is 8 mm away from the MOT. (c) Temperature data of two PT100 platinum resistors located in the BBR shield.

Inside the science chamber, a copper BBR shield provides a uniform and well-characteristic temperature for atoms, as shown in Fig. 1(b). Two apertures (1.00(3) mm diameter) are used to transmit the lattice and clock lasers, where the small-sized aperture minimizes exposure to room-temperature blackbody radiation. The BBR shield also avoids collision between the lattice-trapped atoms and the thermal beam from the oven. A four-stage Peltier cooler attached to the shield's base actively stabilizes its temperature. Two thin-film platinum resistors (PT100) monitor the temperature of the shield. One sensor is near the MOT and the other is near the viewport. The shield is blackened through high-temperature oxidation. The potential temperature gradient in the BBR shield is estimated to be below 1 mK. A polyether-ether-ketone (PEEK) outer layer suppresses radiative and convective thermal coupling. As shown in Fig. 1(c), the shield is temperature controlled to 273.15 K with fluctuation of about ±1.5 mK for an hour, and fluctuation of about 10 mK for measurements over a few days, with the calibration accuracy of the temperature probe being 10 mK.

While reducing the BBR shift, it is also critical to address another major shift of optical lattice clocks, the lattice AC Stark shift. Conventional optical lattices typically employ deep trap depths (typically more than $100E_r$) to suppress the tunnelling. However, this kind of configuration amplifies the lattice AC Stark shifts and reduces coherent time between atoms and interrogation light. To resolve this trade-off, we implement an optical lattice with a 75° angle between the longitudinal direction and gravity to take advantage of the earth's gravity to improve the differentiation between lattice potential sites and obtain the well-known Wannier–Stark states to realize a shallow lattice with minimal tunneling.[20] By means of a hydraulic support bar under the breadboard, the system can be tilted to an arbitrary angle (here the longitudinal direction

of the lattice is at an angle of 75° with respect to gravity).

A 20 L/s ion pump and an ion-gettering pump (containing a 100 L/s getter pump and a 5 L/s ion pump) are used to maintain a pressure of 4×10^{-9} Pa for the oven region. An ion-gettering pump (containing a 75 L/s ion pump and a 300 L/s getter pump) is used for the science chamber region at 2×10^{-8} Pa. A differential tube is set at the junction of these two regions to isolate the two regions.

The optical system contains three optical breadboards used for the first stage of laser cooling (blue MOT), the second stage of laser cooling (red MOT) and the lattice realization, respectively. In this experiment, trapping lights of the blue MOT are provided by the 461 nm laser (TOPTICA SHG-pro), which is delivered to the corresponding optical breadboard by a single-mode polarization-maintaining (SMPM) fiber and its frequency and power distribution in the breadboard are shown in Fig. 2(a). The frequency of the 461 nm laser is locked to the $5s^2\,{}^1S\rightarrow5s5p\,{}^1P_1$ transition of ^{88}Sr by the fluorescence detection method. A laser amplitude stabilizer (Thorlabs NEL01/M) is added to the detection light used for exciting fluorescence during the excitation fraction detection and atom number measurement. Atoms in the $5s5p\,{}^1P_1$ state can leak into the long-lived dark state $5s5p\,{}^3P_2$, reducing the cooling efficiency. Thus, 679 nm (Precilaser) and 707 nm (TOPTICA DL-pro) lights are used to excite $5s5p\,{}^3P\rightarrow5s6s\,{}^3S_1$ and $5s5p\,{}^3P_2\rightarrow5s6s\,{}^3S_1$ transitions, respectively. Atoms can return to the $5s^2\,{}^1S$ ground state through the $5s5p\,{}^3P_1$ state with a short lifetime.

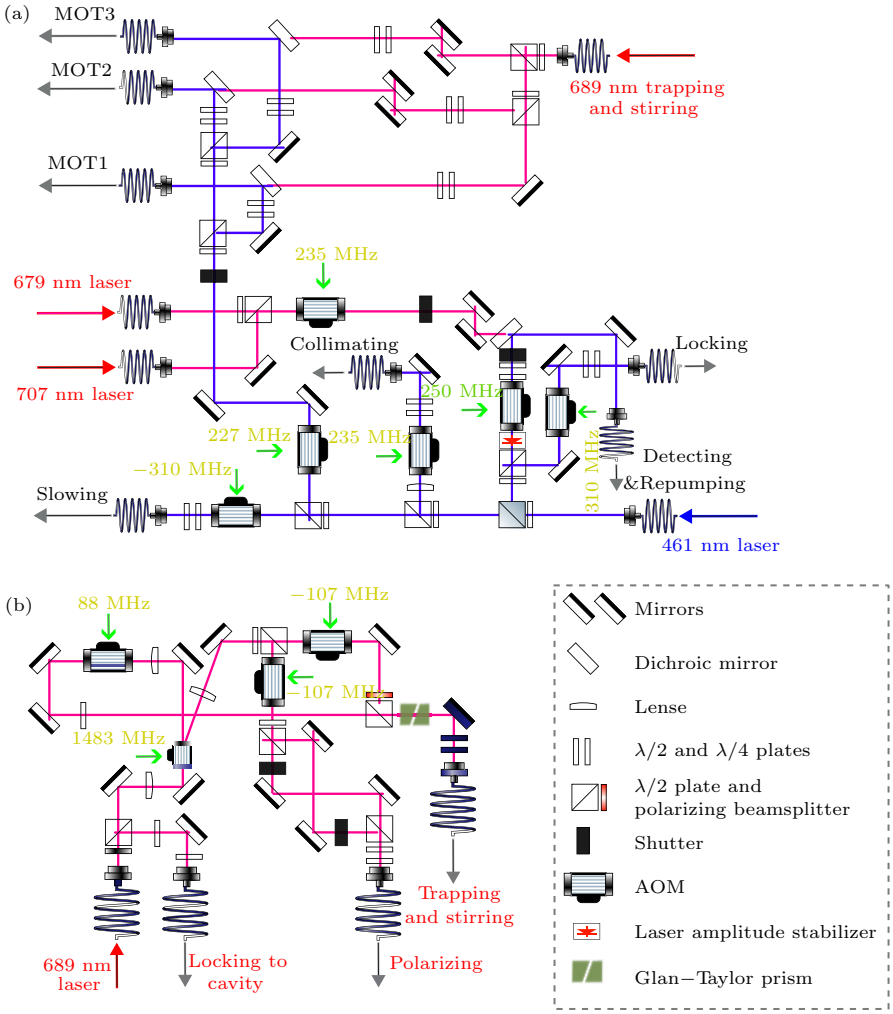


Fig. 2. (a) Optical breadboard used for the blue MOT. Beams pass through acousto-optic modulators (AOMs) with different detuning to satisfy collimating, slowing, trapping and detecting beams. Optical shutters provide sub-microsecond beam blocking for timing control. (b) Optical breadboard used for the red MOT. The 689 nm trapping and stirring beams are then input to the first cooling breadboard, merging with the 461 nm trapping beam to be the laser part of the MOT. Two opposite circular direction polarized beams are used for the state preparation of atoms.

Figure 2(b) shows the optical breadboard for the red MOT, which is based on the $5s^2\,{}^1S\rightarrow5s5p\,{}^3P_1$ transition at 689 nm. The phase of the 689 nm laser (Precilaser) is locked to an ultralow-expansion (ULE) cavity with a fineness of 20000, and its frequency is close to the trapping light of the red MOT corresponding to the $5s^2\,{}^1S\ (F=9/2)\rightarrow5s5p\,{}^3P_1$ $(F=11/2)$ transition. A stirring light, corresponding to $5s^2\,{}^1S$ $(F=9/2)\rightarrow5s5p\,{}^3P_1$ $(F=9/2)$ transition is used for rapid redistribution of atoms among the groundstate Zeeman sublevels, increasing cooling efficiency. The frequency difference of 1.46 GHz between the trapping and stirring lights is achieved by a broadband AOM, instead of our previous injec-

tion locking method. The trapping and stirring lights of the red MOT are combined via the polarizing beamsplitter (PBS), purified by the Glan–Taylor prism, coupled into an SMPM fiber, and finally overlapped with the 461 nm trapping light shown in Fig. 2(a). The polarization light, used for optically pumping atoms into stretched states, is divided by 20% before the AOM of the stirring light. The $m_F = \pm 9/2$ states are realized by applying $\sigma^{\pm}$ polarized lights, which is achieved by switching the two polarization lights with σ^{+} and σ^{-} polarization, respectively. This method can avoid using the liquid crystal waveplate, where two polarizing beams are coupled into the same fiber with orthogonal polarization directions.

The two beams of the lattice laser are frequency shifted via respective AOMs driven by a common digital signal source. As shown in Fig. 3, a high-power fiber laser (Precilaser) generates the lattice light, and a 0.2 nm bandpass filter suppresses background spontaneous radiation.[22] The optical lattice is formed by interfacing the two counter-propagating lattice beams shown in Fig. 4, where the beam diameter of both lattice lights is about 110 μm at the MOT center. A partial reflector with about 4% reflectivity is used to sample the phase difference between two lattice beams detected by an avalanche photodiode (APD) and the differential phase noise after locking is below 4 mrad.[23]

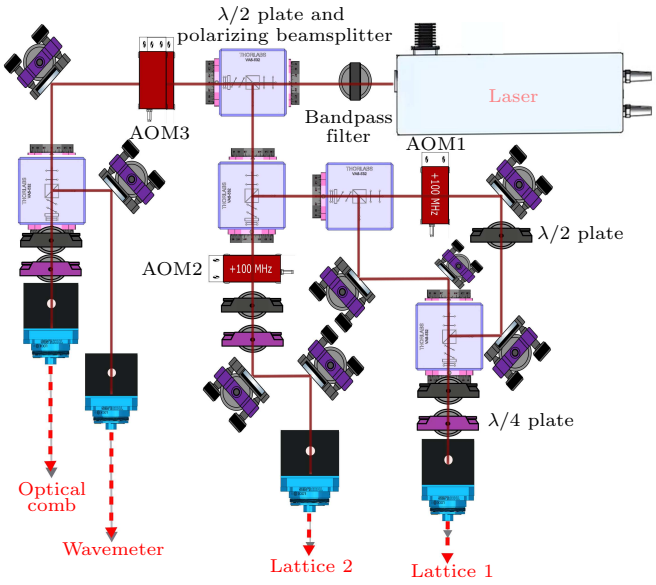


Fig. 3. Schematic diagram of the lattice laser breadboard. Laser is phase locked to the optical comb at the 'magic wavelength'. Lattice 2 contains two orthogonal-polarization beams, where the beam divided before the AOM is the reference light. Relative phase between lattice 1 and lattice 2 beams is locked by intervening the lattice 2 and reference lights and feedbacking the driving frequency of AOM2. AOM1 is used to modulate the frequency of lattice 1 during the moving of the optical lattice stage, inducing a controlled differential detuning between the two lattice beams.

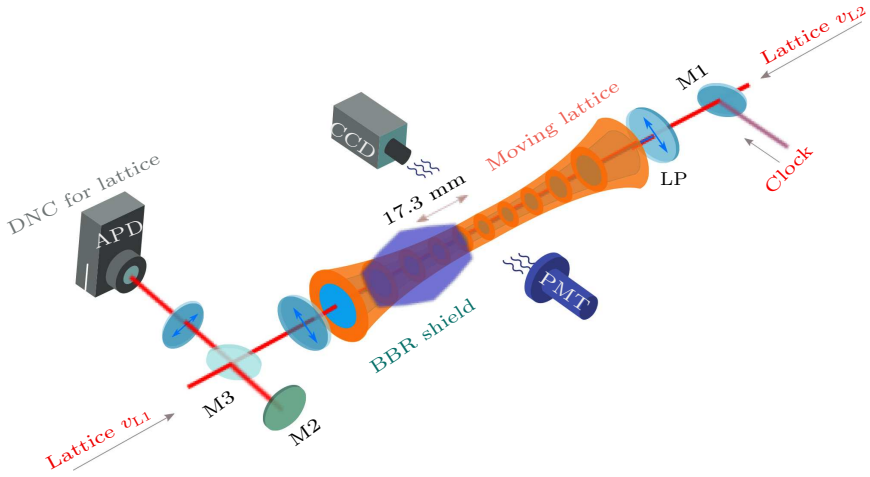


Fig. 4. Polarizations of the clock and lattice lasers are parallel to the quantization axis defined by a bias magnetic field of z-direction Helmholtz coils. Partial reflector mirror (M3) serves as a reference point for the DNC (Doppler noise cancellation) applied to the two lattice beams. LP represents the linear polarizer, M1 is a dichroic mirror, M2 is a zero-degree reflector, and PMT represents the photomultiplier tube.

The clock laser (Precilaser) is frequency-stabilized to a 20 cm long ULE cavity with a finesse of 200000, and the ULE cavity is housed within a precisely temperature-controlled vacuum chamber. The flicker noise floor of the clock laser is determined to be 4×10^{-16}. The clock laser is kept resonant with transition by frequency shifting through the AOM. Timing control is achieved by switching the frequency (detuning at 1 MHz) and avoiding frequency shift and uncertainty due to chirping. The 698 nm laser is delivered into the physics package via the SMPM fiber, and the phase noise of the fiber is suppressed by partially reflecting the laser through the output face of the fiber.

3. Experimental results

3.1. Preparation of atoms

Using the physical system and the optical system described above, we demonstrate full control of ^{87}Sr atoms through the blue MOT, red MOT, state preparation, movable lattice and normalized spectroscopic detection of atoms in the SrII system. Interrogation by clock beam is achieved in the BBR shield. A simple schematic of the timing sequence of the

experiment is shown in Fig. 5 with corresponding EMCCD atomic cloud images displayed above.

The experimental timing sequence initiates with a blue MOT on the $^1S_0 \rightarrow {}^1P_1$ transition. The atomic beam is collimated radially, and then decelerated to ~50 m/s via a Zeeman slower. Finally, the atoms are trapped by the MOT formed by anti-Helmholtz magnetic coils and trapping beams at the center of the science chamber. As shown in Fig. 5, the blue MOT lasts 220 ms, followed by a linear power ramp-down via a variable voltage attenuator to minimize atomic loss from spontaneous emission. During the transfer from the first laser cooling to the second, the atoms are subjected to a relatively weak gradient magnetic field with 689 nm $^1S_0$ $(F = 9/2) \rightarrow {}^3P_1$ $(F = 11/2)$ trapping beams and $^1S_0$ $(F = 9/2) \rightarrow {}^3P_1$ $(F = 9/2)$ stirring beams, and the frequencies of the two beams are subjected to frequency modulation for broad velocity capture.[24] Then magnetic field compression and single-frequency cooling further reduce temperatures to 3 μK.

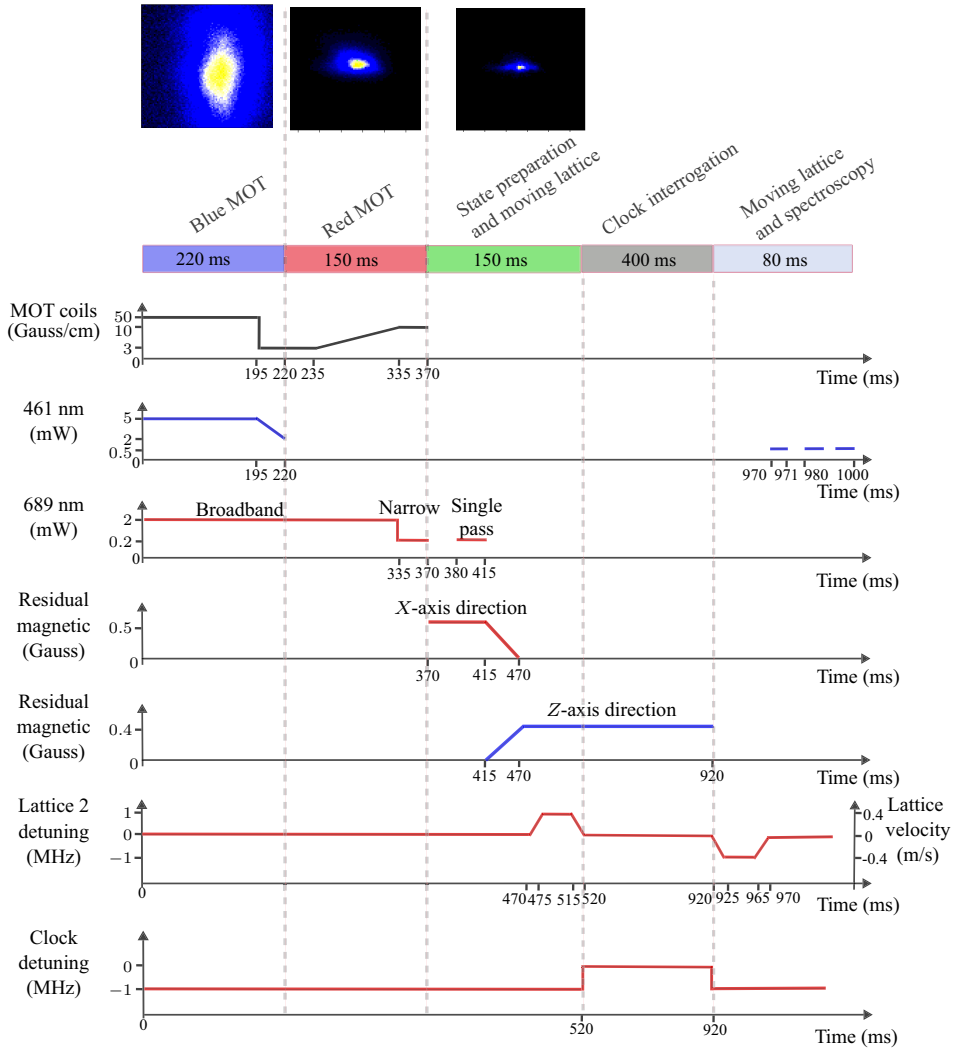


Fig. 5. Schematic of the timing sequence used for the SrII, and corresponding camera images are shown above. Key components of the experimental control, namely, the power of beams at 461 nm and 689 nm, the magnetic field of MOT coils and residual magnetic field at the center of the science chamber, the detuning profiles of the lattice 2 beam and clock beam are synchronized with timing sequence.

At the end of the laser cooling, the atoms are automatically loaded in a 1D optical lattice formed by strictly aligned beams at the magic wavelength. To mitigate thermal radiation shifts, atoms are transported into a BBR shield via a movable lattice. The movable optical lattice is realized by programming the driven frequency of AOM1 in Fig. 3 to induce frequency detuning between the two beams. A conventional optical lattice is a standing wave field with zero detuning, while constant detuning Δf causes the lattice to generate velocity $v = \lambda \Delta f/2$.[25] When the detuning Δf varies linearly with time, the lattice moves with uniform acceleration (deceleration). During the movement of the optical lattice, AOM1 is programmed to update the frequency at very small intervals (< 1 μs) after receiving the command to move the optical lattice to ensure less atom loss during lattice acceleration and deceleration. Optimized acceleration and deceleration profiles retain 50% of atoms after transport. The atoms are then situated in the BBR shield, 10.5(2) mm from the aperture, as inferred from the CCD image and BBR shield dimensions.

In order to obtain high-excitation spectra, we choose $^1S_0$ $(m_F = +9/2) \rightarrow {}^3P_0$ $(m_F = +9/2)$ and $^1S_0$ $(m_F = -9/2) \rightarrow {}^3P_0$ $(m_F = -9/2)$ as the reference for closed-loop locking, and

thus need to pump the atoms to the corresponding Zeeman sublevels using a 689 nm $^1S_0$ ($F = 9/2$)–$^3P_1$ ($F = 9/2$) polarizing beam. The traditional method is to apply a bias magnetic field in the direction of the quantization axis of the system (the z-axis of the science chamber in Fig. 1) to complete the state preparation, which requires the addition of mechanical shutters and liquid crystal waveplates to ensure single pass and switch of the polarizing beam. In this experiment, we add two additional polarizing beams, and the beams are incident from the viewport for the slowing beam in the x-axis direction. In the state preparation of polarization, the residual magnetic field in the x-axis is first added to complete the state preparation of the atoms in conjunction with the corresponding polarizing beam. Then, the amplitude of the x-axis magnetic field is linearly decreased, while the magnetic field in the z-axis is linearly increased to complete the rotation of the quantization axis so that it is consistent with the polarization direction of the lattice beam and clock beam.

After completing the excitation of the atoms in the BBR shield, the atoms are moved back to the center of the science chamber using the same frequency modulation method, and three short pulses of 461 nm detecting beams are used to complete the normalized detection of the excitation fraction of the atoms. The atomic fluorescence is collected by PMT.

3.2. Spectroscopy and stability

Using the experimental setup and timing sequence described above, we observe a spectrum with resolved sidebands and narrow linewidth, as shown in Figs. 6(a) and 6(b). After energy filtering to remove hotter atoms,[26] the lattice potential is set to be $40E_r$ with about 1000 atoms interrogated by clock laser.[27] The temperature of the atoms is about 2 μK, obtained by fitting the blue sidebands. Further linewidth narrowing to 2.5 Hz is achieved through clock laser power optimization and residual magnetic field compensation.

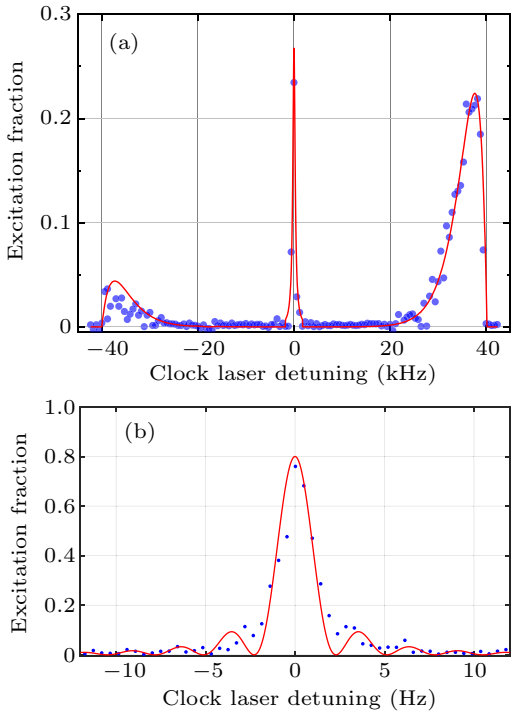


Fig. 6. Clock transition spectra. (a) Spectrum having motional sidebands for $U_0 = 40E_r$. (b) High-resolution spectrum with a 400 ms clock pulse (indicating a Fourier limited linewidth of 2.2 Hz).

The stability of the system has been measured using the self-comparison method, where two independent digital servo loops are used to lock the frequency of the clock laser at the half-height width of the spectroscopy, and the self-comparison stability of the system is $(\nu_1 - \nu_2)/\sqrt{2}$, where ν_1 and ν_2 are the clock transition frequencies obtained after the two servo locks.[3,28,29] As shown in Fig. 7, the fitting line yields a self-comparison stability of $5.1 \times 10^{-16}(\tau/\mathrm{s})^{-0.5}$.

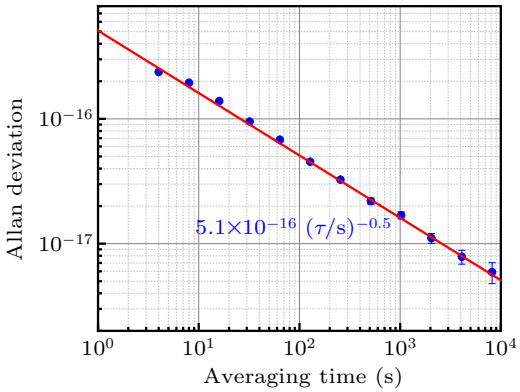


Fig. 7. Allan deviation of the frequency difference between two interleaved atomic servos. Red fitting line indicates the interleaved instability of $5.1 \times 10^{-16}(\tau/\mathrm{s})^{-0.5}$.

4. Conclusion and perspectives

The SrII optical lattice clock developed at the NTSC represents a significant advancement in optical lattice clock technology through innovative design and precision engineering. Key enhancements include a temperature-controlled BBR shield (10 mK stability), a shallow optical lattice with suppressed tunneling, and phase-stabilized counter-propagating lattice beams. The implementation of a movable optical lattice enabled atom transport into the BBR shield. In addition, the novel polarization method can simplify the system. Conductive vacuum viewports minimized DC Stark shifts, further enhancing clock accuracy.

This study not only advances the roadmap for redefining the SI second but also expands capabilities for precision tests of fundamental physics, including gravitational redshift measurements and searches for dark matter. Future efforts will focus on improving long-term stability, completing the measurement of the total systematic uncertainty, and multi-clock comparisons for the absolute frequency measurement. By reducing systematic uncertainties below 1×10^{-18}, this platform will position itself as a pivotal tool in both metrology and fundamental physics exploration.

Acknowledgements

This study is supported by the Innovation Program for Quantum Science and Technology (Grant Nos. 2021ZD0300900 and 2021ZD0300902), the Strategic Priority Research Program of the Chinese Academy of Sciences (Grant No. XDB35010202), and the Operation and Maintenance of Major Scientific and Technological Infrastructure of the Chinese Academy of Sciences (Grant No. 2024000014).

References

[1] Ludlow A D, Boyd M M, Ye J, Peik E and Schmidt P O 2015 *Rev. Mod. Phys.* **87** 637
[2] McGrew W F, Zhang X, Fasano R J, Schaffer S A, Beloy K, Nicolodi D, Brown R C, Hinkley N, Milani G, Schioppo M, Yoon T H and Ludlow A D 2018 *Nature* **564** 87
[3] Brewer S M, Chen J S, Hankin A M, Clements E R, Chou C W, Wineland D J, Hume D B and Leibrandt D R 2019 *Phys. Rev. Lett.* **123** 033201
[4] Oelker E, Hutson R B, Kennedy C J, Sonderhouse L, Bothwell T, Goban A, Kedar D, Sanner C, Robinson J M, Marti G E, Matei D G, Legero T, Giunta M, Holzwarth R, Riehle F, Sterr U and Ye J 2019 *Nat. Photonics* **13** 714
[5] Aeppli A, Kim K, Wareld W, Safronova M S and Ye J 2024 *Phys. Rev. Lett.* **133** 023401
[6] Filzinger M, Dorscher S, Lange R, Klose J, Steinel M, Benkler E, Peik E, Lisdat C and Huntemann N 2023 *Phys. Rev. Lett.* **130** 253001
[7] Boulder Atomic Clock Optical Network BACON Collaboration 2021 *Nature* **591** 564
[8] Takamoto M, Ushijima I, Ohmae N, Yahagi T, Kokado K, Shinkai H and Katori H 2020 *Nat. Photonics* **14** 411
[9] Zheng X, Dolde J, Cambria M C, Lim H M and Kolkowitz S 2023 *Nat. Commun.* **14** 4886
[10] Dimarcq N, Gertsvolf M, Mileti G, *et al.* 2024 *Metrologia* **61** 012001
[11] Riehle F, Gill P, Arias F and Robertsson L 2018 *Metrologia* **55** 188
[12] Lodewyck J 2019 *Metrologia* **56** 055009
[13] Ushijima I, Takamoto M, Das M, Ohkubo T and Katori H 2015 *Nat. Photonics* **9** 185
[14] Bothwell T, Kedar D, Oelker E, Robinson J M, Bromley S L, Tew W L, Ye J and Kennedy C J 2019 *Metrologia* **56** 065004
[15] Lu B K, Sun Z, Yang T, Lin Y G, Wang Q, Li Y, Meng F, Lin B K, Li T C and Fang Z J 2022 *Chin. Phys. Lett.* **39** 080601
[16] Lu X T, Guo F, Wang Y B, Xu Q F, Zhou C H, Xia J J, Wu W J and Chang H 2023 *Metrologia* **60** 015008
[17] Li J, Cui X Y, Jia Z P, *et al.* 2024 *Metrologia* **61** 015006
[18] Beloy K, Hinkley N, Phillips N B, Sherman J A, Schioppo M, Lehman J, Feldman A, Hanssen L M, Oates C W and Ludlow A D 2014 *Phys. Rev. Lett.* **113** 260801
[19] Kim K, Aeppli A, Bothwell T and Ye J 2023 *Phys. Rev. Lett.* **130** 113203
[20] Lemonde P and Wolf P 2005 *Phys. Rev. A* **72** 033409
[21] Beloy K, Zhang X, McGrew W F, Hinkley N, Yoon T H, Nicolodi D, Fasano R J, Scha er S A, Brown R C and Ludlow A D 2018 *Phys. Rev. Lett.* **120** 183201
[22] Jia Z P, Cui X Y, Xie Y J, Zhang X, Niu G Z, Liu X Y, Zhu Q Q, Li J and Dai H N 2025 *Phys. Rev. Appl.* **23** 014014
[23] Falke S, Misera M, Sterr U and Lisdat C 2012 *Appl. Phys. B* **107** 301
[24] Katori H, Ido T, Isoya Y and Kuwata-Gonokami M 1999 *Phys. Rev. Lett.* **82** 1116
[25] Zheng X, Dolde J, Lochab V, Merriman B N, Li H and Kolkowitz S 2022 *Nature* **602** 425
[26] Baillard X, FouchéM, Targat R L, Westergaard P G, Lecallier A, Chapelet F, Abgrall M, Rovera G D, Laurent P, Rosenbusch P, Bize S, Santarelli G, Clairon A, Lemonde P, Grosche G, Lipphardt B and Schnatz H 2008 *Eur. Phys. J. D* **48** 11
[27] Blatt S, Thomsen J W, Campbell G K, Ludlow A D, Swallows M D, Martin M J, Boyd M M and Ye J 2009 *Phys. Rev. A* **80** 052703
[28] Al-Masoudi A, Dorscher S, Hafner S, Sterr U and Lisdat C 2015 *Phys. Rev. A* **92** 063814
[29] Santarelli G, Audoin C, Makdissi A, Laurent P, Dick G and Clairon A 1998 *IEEE Trans. Ultrason. Ferroelectr. Freq. Control* **45** 887
[30] Bothwell T, Kennedy C J, Aeppli A, Kedar D, Robinson J M, Oelker E, Staron A and Ye J 2022 *Nature* **602** 420